Methylidyne Cavity Ring-Down Spectroscopy in a Microwave Plasma Discharge

László Nemes [1], Christian G. Parigger [2],*

[1] Research Center for Natural Sciences, Institute for Materials and Environmental Chemistry, 1117 Budapest, Magyar tudósok körútja 2, Hungary; nemesl@chemres.hu

[2] Physics and Astronomy Department, University of Tennessee, University of Tennessee Space Institute, Center for Laser Applications, 411 B.H. Goethert Parkway, Tullahoma, TN 37388-9700, USA; cparigge@tennessee.edu; Tel.: +1-(931)-841-5690

* Correspondence: cparigge@tennessee.edu;

Abstract: This work communicates cavity ring-down spectroscopy (CRDS) of methylidyne (CH) in a chemiluminescent plasma that is produced in a microwave cavity. Of interest are the rotational lines of the 0-0 vibrational transition for the A-X band and the 1-0 vibrational transition for the B-X band. The reported investigations originate from CH-radical research in 1996 that constituted the first case of applying CRDS to the CH radical. The report also includes recent analysis that shows excellent agreement of measured and computed data, and it communicates CH line strength data.

Keywords: molecular spectroscopy; diatomic molecules; cavity ring-down spectroscopy; absorption spectroscopy; methylidyne; line strength data; plasma physics; astrophysics

1. Introduction

Cavity ring-down spectroscopy (CRDS) was introduced by O'Keefe and Deacon in 1988 [1] and has since been used to an increasing extent for the measurement of weak absorbers or minute amounts of substances in the gaseous phase. Thus overtone bands [2] and the Herzberg absorption system in molecular oxygen [3] have been analyzed this way. Jet-cooled metal clusters [4,5] and trace gas components [6] were probed by CDRS. Additionally, CDRS has proved eminently applicable for chemical kinetic system analysis, e.g., see Refs. [7,8], that often involve transient radicals. Free radicals such as oxymethyl (HCO) in hydrocarbon flames [9] or the methyl (CH_3) radical [10] were studied by this technique. We have applied this method in the form of coherent CRDS [11] to the spectroscopic analysis of the mehylidyne (CH) radical.

This report communicates selected data records from investigations in 1996. Specifically, the CH B-X transition has been subject research in subsequent years [12–14]. In addition, this report summarizes recent analysis that utilizes accurate line strength data for CH [15,16], and provides the CH line strength data for the A-X and B-X transitions. The line strength files (LSFs) for CH can also be applied for analysis of emission spectra that may be collected in laser-induced breakdown spectroscopy [17,18]. The work in this report may have applications in astrophysics [19–21], combustion studies [22] and diamond film chemical vapor deposition [23].

2. Materials and Methods

2.1. Experiment Details

The CH radicals were generated by the oxydation of acetylene (C_2H_2) using excited oxygen atoms produces in an inductively coupled microwave plasma (200 W at 2.45 GHz) in oxygen gas bubbled through water. The discharge was initiated in argon employing a flow inlet a few centimeters from the cavity mirrors. The flow of argon suppressed etching of the coating of the reflective mirrors by the flow of radicals. The chemiluminescent

reaction leading to the generation of CH in the CDRS cavity occurred upon mixing the
wet oxygen and acetylene via a distributed set of inlet openings, while the cavity was
continuously pumped by two Roots pumps of a total capacity of 500 m³/hour. This
source was previously described by Ubachs *et al.* [24] The total pressure of the reactive gas
mixture (Ar, O_2, C_2H_2 and water vapor) was kept at 400 Pa (3 Torr), as this provided the
optimum setting for the CRDS signals. The CDRS mirrors had reflectivities of $R_1 = 0.993$
and $R_2 = 0.997$, in the 363-nm to 430-nm range.

2.2. Diatomic Spectra Computation Details

The computations of the A-X and B-X transitions of CH rely on establishment of
an accurate line strengths. For analysis of the measured CH transitions, two sets of line
strength files are communicated as supplement to this work. The development of line
strength data is discussed with specific details for the C_2 Swan bands, computation of
laser-induced fluorescence- and absorption- spectra [15]. The line strengths for diatomic
molecules follows recently published procedures [16]. Several applications in the analysis
of optical breakdown spectra are communicated [16–18], including data files and the
two programs (i) Boltzmann equilibrium spectrum program (BESP) and Nelder-Mead
temperature (NMT), for analysis of selected diatomic molecules [25].

Tables 1 and 2 communicate excerpts of the set of line strength data applicable for
analysis of recorded CRDS data. These data files can be conveniently utilized with BESP
and NMT, see Ref. [25]. For computation of emission spectra in the analysis of laser-plasma,
only the wave number, upper term value, and line strengths are needed. For computation
of emission spectra [18], MATLAB [26] source code[27] has been made available recently.
However, for computation of absorption spectra, the lower term values are required.
The collated CH data files in Tabs. 1 and 2 also show standard designations for diatomic
molecules [28].

3. Results and Discussion

An overview emission spectrum for CH A-X illustrates the wavelength range of the
provided line strength data. Figure 1 shows $\Delta v = 0$ transitions for v′ = v″ = 0, 1, 2. An
instrument resolution, $\delta\lambda$, of $\delta\lambda = 0.05$ nm is selected, and an equilibrium temperature,
T, is set to 3.0 kK. Such a spectrum may apply to analysis of laser-plasma emission. Fig. 2
displays computed CH B-X spectra for $\Delta v = 0, +1$ transition, i.e., v′ = v = 0, 1, and v′ = 1 to
v″ = 0.
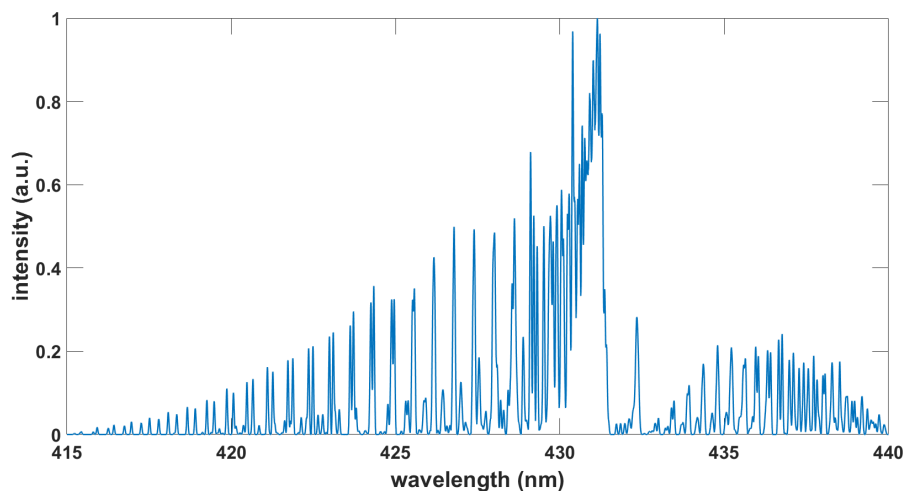
Figure 1. Computed CH A-X spectrum, $\Delta v = 0$, $\delta\lambda = 0.05$ nm, T = 3.0 kK.

Table 1. First two dozen of 1384 lines for the CH $A\,^2\Delta \leftrightarrow X\,^2\Pi$ line strength table with column headings: J' upper and J'' lower total angular momentum quantum number (nuclear spin not included); P_{ij}, or Q_{ij}, or R_{ij}, line designation based on J', J'', $F_{J'}$, $F_{J''}$; v' upper and v'' lower vibrational quantum number; p' upper and p'' lower parity designations, the $\pm$ total parity eigenvalue is followed by the e/f parity; N' upper and N'' lower total orbital angular momentum quantum number; $F_{J'}$ upper and $F_{J''}$ Lower term value computed from model Hamiltonian, cm^{-1}; $\tilde{\nu}$ vacuum wavenumber, $\tilde{\nu} = F_{J'} - F_{J''}$, cm^{-1}; $S_{J'J''}$ Hönl-London term, unitless; $S_{n'v'J'n''v''J''}$ line strength, stC^2 cm^2 (1 stC = 3.356×10^{-10} C).

J'	J''		v'	v''	p'	p''	N'	N''	$F_{J'}$	$F_{J''}$	$\tilde{\nu}$	$S_{J'J''}$	$S_{S_{n'v'J'n''v''J''}}$
1.5	2.5	P22	0	0	+f	-f	2	3	24663.5612	1569.6083	23093.9531	0.2013	0.8026
1.5	2.5	P21	0	0	+f	-f	2	2	24663.5612	1489.0759	23174.4844	0.1996	0.7973
1.5	2.5	P11	0	0	-e	+e	1	2	24663.5612	1489.2381	23174.3223	0.2004	0.8001
1.5	2.5	P12	0	0	-e	+e	1	3	24663.5612	1569.1156	23094.4453	0.2005	0.7986
1.5	1.5	Q21	0	0	+f	-e	2	1	24663.5612	1433.8288	23229.7324	0.7998	3.200
1.5	1.5	Q22	0	0	+f	-e	2	2	24663.5612	1482.8608	23180.7012	0.8038	3.211
1.5	1.5	Q12	0	0	-e	+f	1	2	24663.5612	1483.1056	23180.4551	0.8075	3.224
1.5	1.5	Q11	0	0	-e	+f	1	1	24663.5612	1433.8051	23229.7559	0.7963	3.184
1.5	0.5	R22	0	0	+f	-f	2	1	24663.5612	1416.0299	23247.5312	2.005	8.020
1.5	0.5	R11	0	0	-e	+e	1	0	24663.5612	1415.9191	23247.6426	2.005	8.021
2.5	3.5	P12	0	0	-f	+f	2	4	24661.8291	1683.5813	22978.2480	0.0070179	0.027893
2.5	3.5	P11	0	0	-f	+f	2	3	24661.8291	1573.3187	23088.5098	0.3709	1.478
2.5	3.5	P21	0	0	+e	-e	3	3	24750.4863	1573.6950	23176.7910	0.2022	0.8070
2.5	3.5	P22	0	0	+e	-e	3	4	24750.4863	1682.7661	23067.7207	0.5651	2.248
2.5	3.5	P22	0	0	-f	+f	3	4	24750.4863	1683.5813	23066.9043	0.5666	2.254
2.5	3.5	P21	0	0	-f	+f	3	3	24750.4863	1573.3187	23177.1680	0.2009	0.8017
2.5	3.5	P11	0	0	+e	-e	2	3	24661.8291	1573.6950	23088.1348	0.3707	1.478
2.5	3.5	P12	0	0	+e	-e	2	4	24661.8291	1682.7661	22979.0625	0.0072268	0.028723
2.5	2.5	Q11	0	0	-f	+e	2	2	24661.8291	1489.2381	23172.5918	1.738	6.944
2.5	2.5	Q12	0	0	-f	+e	2	3	24661.8291	1569.1156	23092.7129	0.1448	0.5773
2.5	2.5	Q22	0	0	+e	-f	3	3	24750.4863	1569.6083	23180.8789	2.093	8.354
2.5	2.5	Q21	0	0	+e	-f	3	2	24750.4863	1489.0759	23261.4102	0.4911	1.964
2.5	2.5	Q21	0	0	-f	+e	3	2	24750.4863	1489.2381	23261.2480	0.4952	1.980
2.5	2.5	Q22	0	0	-f	+e	3	3	24750.4863	1569.1156	23181.3711	2.089	8.335

Table 2. First two dozen of 261 lines for the CH $B\,^2\Sigma^- \leftrightarrow X\,^2\Pi$ line strength table with column headings (identical to the ones in Table 1).

J'	J''		v'	v''	p'	p''	N'	N''	$F_{J'}$	$F_{J''}$	$\tilde{\nu}$	$S_{J'J''}$	$S_{n'v'J'n''v''J''}$
0.5	1.5	P11	0	0	-f	+f	0	1	27114.2564	1433.9116	25680.3457	2.498	0.2572
0.5	1.5	P12	0	0	-f	+f	0	2	27114.2564	1483.2126	25631.0430	0.1750	0.018018
0.5	1.5	P22	0	0	+e	-e	1	2	27139.5581	1482.9686	25656.5898	2.493	0.2567
0.5	1.5	P21	0	0	+e	-e	1	1	27139.5581	1433.9356	25705.6230	0.1802	0.018552
0.5	0.5	Q11	0	0	-f	+e	0	0	27114.2564	1416.0057	25698.2500	1.337	0.1376
0.5	0.5	Q21	0	0	+e	-f	1	0	27139.5581	1416.1159	25723.4414	1.337	0.1376
1.5	2.5	P11	0	0	+f	-f	1	2	27139.5166	1489.1826	25650.3340	3.508	0.3612
1.5	2.5	P12	0	0	+f	-f	1	3	27139.5166	1569.7157	25569.8008	0.1008	0.010374
1.5	2.5	P22	0	0	-e	+e	2	3	27190.0681	1569.2245	25620.8438	3.505	0.3609
1.5	2.5	P21	0	0	-e	+e	2	2	27190.0681	1489.3449	25700.7227	0.1032	0.010624
1.5	1.5	Q12	0	0	+f	-e	1	2	27139.5166	1482.9686	25656.5488	0.019638	0.0020218
1.5	1.5	Q11	0	0	+f	-e	1	1	27139.5166	1433.9356	25705.5801	3.723	0.3833
1.5	1.5	Q21	0	0	-e	+f	2	1	27190.0681	1433.9116	25756.1562	0.017592	0.0018112
1.5	1.5	Q22	0	0	-e	+f	2	2	27190.0681	1483.2126	25706.8555	3.725	0.3835
1.5	0.5	R11	0	0	+f	-f	1	0	27139.5166	1416.1159	25723.4004	0.6683	0.068806
1.5	0.5	R21	0	0	-e	+e	2	0	27190.0681	1416.0057	25774.0625	0.6683	0.068803
2.5	3.5	P11	0	0	-f	+f	2	3	27189.9989	1573.4256	25616.5742	4.511	0.4645
2.5	3.5	P12	0	0	-f	+f	2	4	27189.9989	1683.6892	25506.3105	0.070992	0.0073091
2.5	3.5	P22	0	0	+e	-e	3	4	27265.6964	1682.8762	25582.8203	4.510	0.4643
2.5	3.5	P21	0	0	+e	-e	3	3	27265.6964	1573.8017	25691.8945	0.072257	0.0074393
2.5	2.5	Q11	0	0	-f	+e	2	2	27189.9989	1489.3449	25700.6543	5.838	0.6010
2.5	2.5	Q22	0	0	+e	-f	3	3	27265.6964	1569.7157	25695.9805	5.838	0.6011
2.5	1.5	R11	0	0	-f	+f	2	1	27189.9989	1433.9116	25756.0879	1.494	0.1538
2.5	1.5	R12	0	0	-f	+f	2	2	27189.9989	1483.2126	25706.7871	0.1099	0.011316
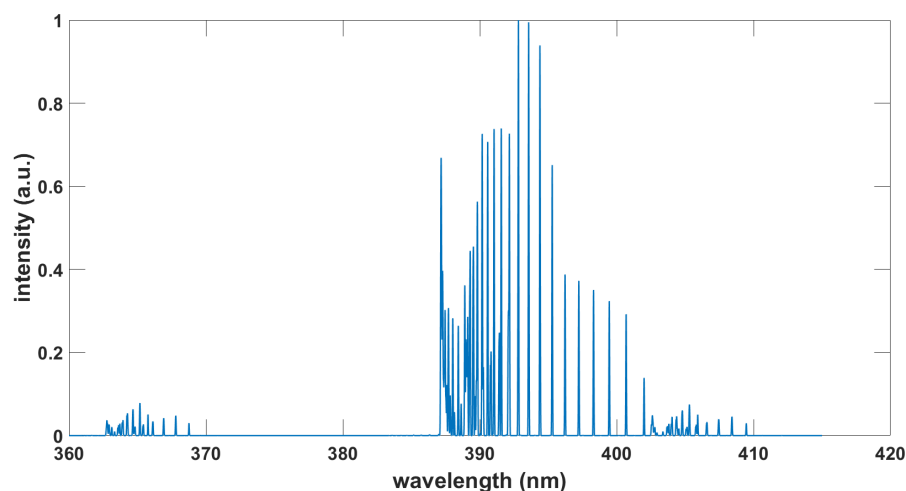
Figure 2. Computed CH B-X spectrum, $\Delta v = 0, +1$, $\delta\lambda = 0.05$ nm, T = 3.0 kK.

For cavity ring-down experiments, a Continuum model-TDL60 Nd:YAG-pumped dye laser was employed. The A-X transition access was accomplished with Coumarin 120 dye that shows a gain maximum of 440 nm. The B-X transition was reached by frequency doubling the output using Styryl 7 dye that shows a gain maximum at 720 nm, or frequency doubled at 360 nm. The available output power ranged from 5 to 15 mJ per pulse, but it was attenuated with diaphragms for CRDS. Overview spectra were initially observed in emission using a low resolution Jobin-Yvon grating spectrometer. Methylidyne A-X bands were noticed near 430 nm that were stronger than the B-X bands near 390 nm, see Figures 1 and 2. In addition, C_2 Swan bands were observed near 470 nm, 520 nm, and 560 nm, e.g., see Ref. [25]. Figure 3 illustrates comparison of measured and fitted absorption spectra.
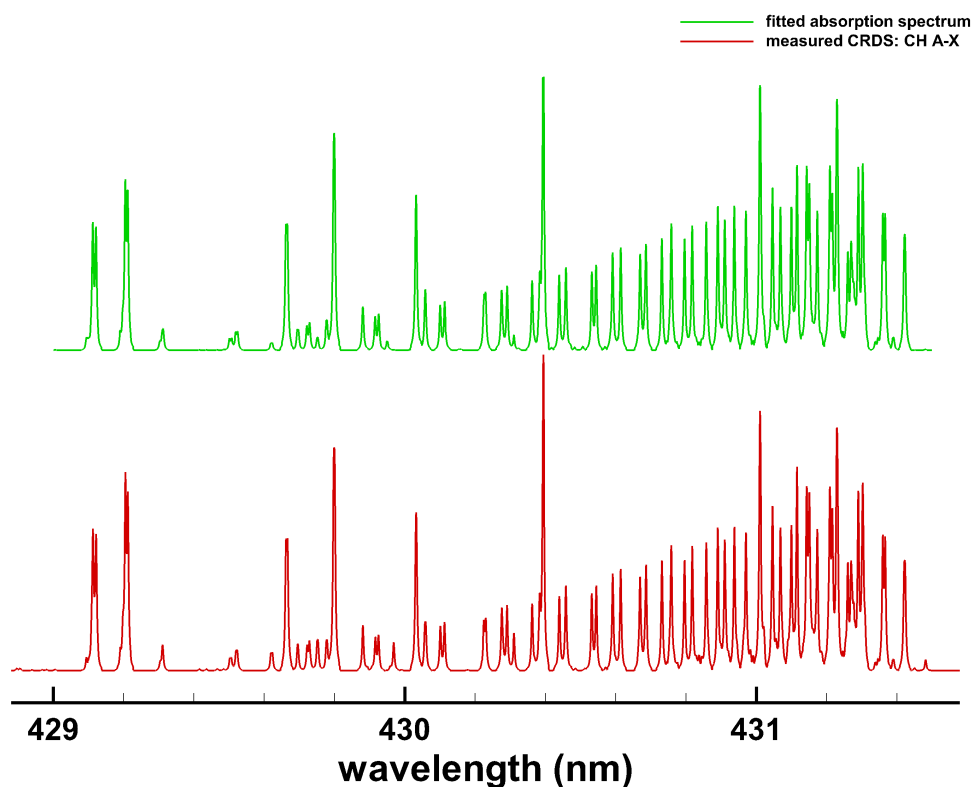
Figure 3. Comparison of measured and fitted CH A-X spectra, $\delta\lambda = 0.005$ nm, T = 1.47 kK.

Figure 4 displays original CRDS data of normalized absorption in the wavenumber range of $23160\,\mathrm{cm}^{-1}$ (431.779 nm) to $23320\,\mathrm{cm}^{-1}$ (428.816 nm). For completeness, Fig. 5 illustrates computed emission spectra in the same vacuum wavenumber range as for Fig. 4. As expected, there are subtle differences for comparisons of absorption spectra, see Fig. 3, or for comparison of CRDS data (Fig. 4) with emission spectra (Fig. 5) that are seen in emission from plasma.
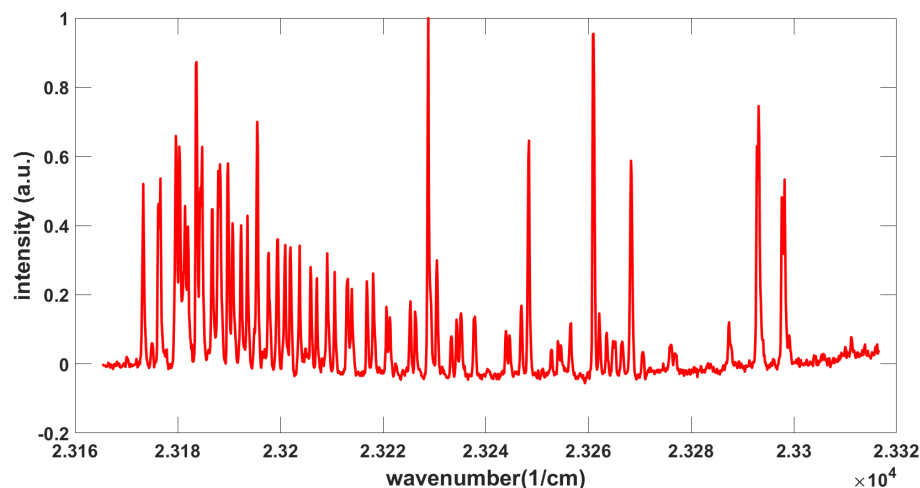
Figure 4. Originally recorded CH A-X spectrum using CRDS.
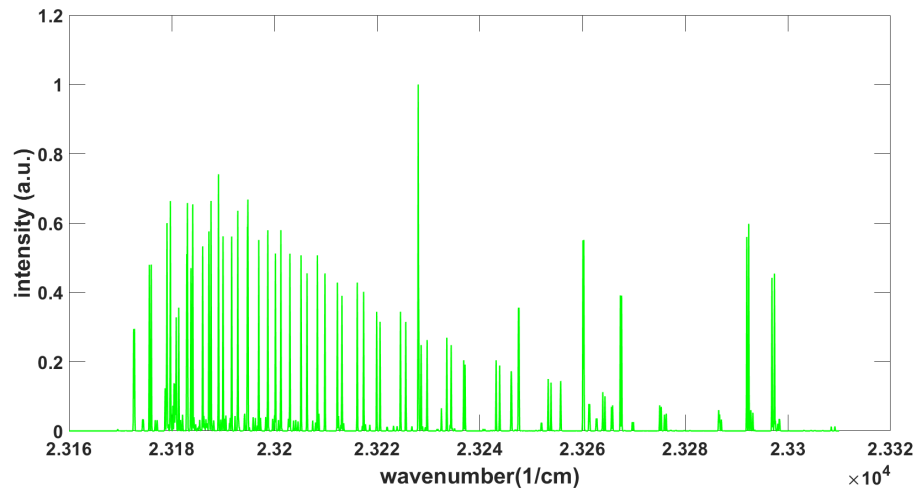
Figure 5. Computed CH A-X emission spectrum, $\delta\tilde{v} = 0.1\,\mathrm{cm}^{-1}$, T = 1.5 kK.

Figure 6 displays an originally recorded B-X CH spectrum, and Fig. 7 shows an emission spectrum for the same vacuum wavenumber range of $27400\,\mathrm{cm}^{-1}$ (364.964 nm) to $27470\,\mathrm{cm}^{-1}$ (364.033 nm).
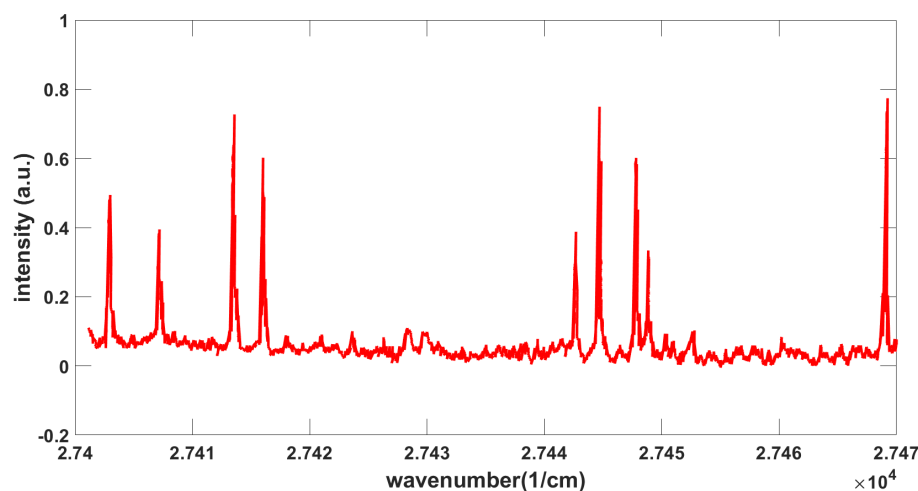
Figure 6. Originally recorded CH B-X spectrum using CRDS.
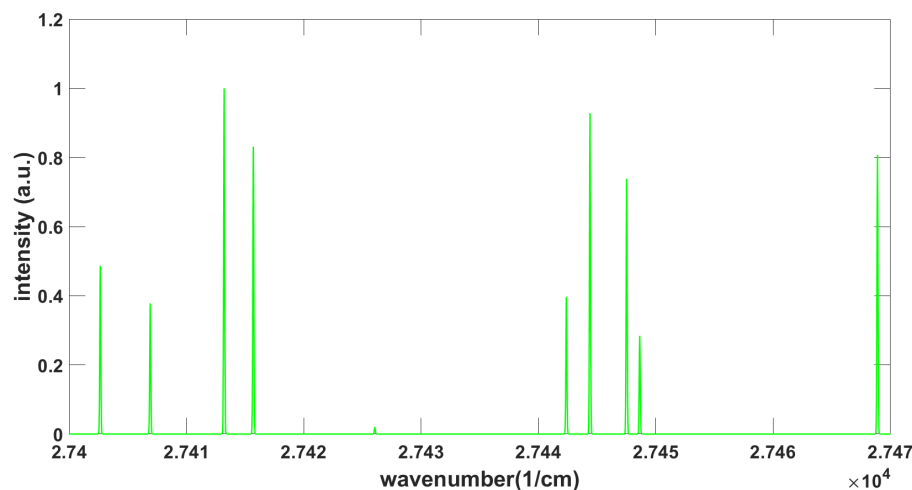
Figure 7. Computed CH B-X emission spectrum, $\delta\tilde{\nu} = 0.1\,\text{cm}^{-1}$, T = 1.5 kK.

4. Conclusions

This work communicates a convincing comparison of recorded cavity ring-down spectra and of computed CH A-X absorption spectra using line strength data. Higher resolution for the investigated CH B-X transition than for the CH A-X transition also confirms reasonable accuracy of measured and computed line positions. Emission spectra of CH A-X and B-X were observed but focus of this work was the application of CRDS for the CH radical. However, the provided line strength data are expected to be useful in emission spectroscopy of plasma that contains hydrocarbons.

Funding: This research received no specific grant-number external funding.

Acknowledgments: CGP acknowledges support in part the State of Tennessee funded Center for Laser Applications at the University of Tennessee Space Institute. LN acknowledges a short term visiting scientist support from the Nederlandse Organistie voor Wetenschappelijk (NWO), as well as support from the Hungarian Research Fund (OTK #3079) for computational equipment in Hungary during the initial research analysis in 1996. Last but not least, LN and CGP acknowledge the consent of Professor Hans J.J. ter Meulen (University of Nijmegen, The Netherlands) to publishing the so far unpublished original material and CRDS data.

Institutional Review Board Statement: Not applicable.

Informed Consent Statement: Not applicable.

Data Availability Statement: Not applicable. [104]

Conflicts of Interest: The authors declare no conflict of interest. The funders had no role in the design [105] of the study; in the collection, analyses, or interpretation of data; in the writing of the manuscript, [106] or in the decision to publish the results. [107]

Abbreviations [108]

The following abbreviations are used in this manuscript: [109]

[110]

BESP	Boltzmann equilibrium spectrum program
CH	methylidyne
CGP	Christian Gerhard Parigger
CRDS	cavity ring-down spectroscopy
LIBS	laser-induced breakdown spectroscopy
LSF	line strength file
LN	László Nemes
Nd:YAG	neodymium-doped yttrium aluminium garnet
NMT	Nelder-Mead temperature
HCO	oxymethyl

[111]

References [112]

1. O'Keefe, A.; Deacon, D.A.G. Cavity ring-down optical spectrometer for absorption measurements using pulsed laser sources. *Rev.* [113] *Sci. Instrum.* **1988**, *59*, 2544–2554. [114]
2. Romanini, D.; Lehmann, K.K. Ring-down cavity absorption spectroscopy of the very weak HCN overtone bands with six, seven, [115] and eight stretching quanta. *J. Chem. Phys* **1993**, *99*, 6287–6301. [116]
3. Huestis, D.L.; Copeland, R.A.; Knutsen, K.; Slanger, T.G.; Jongma, R.T.; Boogaarts, M.G.H.; Meijer, G. Branch intensities and [117] oscillator strengths for the Herzberg absorption systems in oxygen. *Can. J. Phys.* **1994**, *72*, 1109–1121. [118]
4. Scherer, J.J.; Paul, J.B.; Collier, C.P.; Saykally, R.J. Cavity ringdown laser absorption spectroscopy and time-of-flight mass [119] spectrometry of jet-cooled copper silicides. *Chem. Phys. Lett.* **1995**, *102*, 5190–5199. [120]
5. O'Keefe, A.; Scherer, J.J.; Cooksy, A.L.; Sheeks, R.; Heath, J.; Saykally, R.J. Cavity ring down dye laser spectroscopy of jet-cooled [121] metal clusters: Cu_2 and Cu_3.*Chem. Phys. Lett.* **1990**, *172* 214–218. [122]
6. Jongma, R.T.; Boogaarts, M.G.H.; Holleman, I.; Meijer, G. Trace gas detection with cavity ring down spectroscopy. *Rev. Sci.* [123] *Instrum.* **1995**, *66*, 2821–2828. [124]
7. Yu, T.; Lin, M.C. Kinetics of phenyl radical reactions studied by cavity-ring-down spectroscopy method. *J. Am. Chem. Soc.* **1993**, [125] *115*, 4371–4372. [126]
8. Yu, T.; Lin, M.C. Kinetics f the C_6H_5 + CCl_4 Reaction in the Gas Phase: Comparison with Liquid-Phase Data. *J. Phys. Chem.* **1994**, [127] *98*, 9697–9699. [128]
9. Cheskis, S. Intracavity laser absorption spectroscopy detection of HCO radicals in atmospheric hydrocarbon flames. *J. Chem.* [129] *Phys.* **1995**, *102*, 1851–1854. [130]
10. Zalicki, P.; Ma, Y.; Zare, R.N.; Wahl, E.H.; Dadamino, J.R.; Owano, T.G.; Kruger, C.H. Methyl radical measurement by cavity [131] ring-down spectroscopy. *Chem. Phys. Lett.* **1995**, *234*, 269–274. [132]
11. Meijer, G.; Boogaarts, M.G.H.; Jongma, R.T.; Parker, D.H.; Wodtke, A.M. Coherent cavity ring down spectroscopy. *Chem. Phys.* [133] *Lett.* **1994**, *217*, 112–116. [134]
12. Wang, C.-C.; Nemes, L.; Lin, K.-C. New onservations on the B state of the CH radical from UV multiphoton dissociation of ketene. [135] *Chem. Phys. Lett.* **1995**, *245*, 585–590. [136]
13. Nemes, L.; Szalay, P.G. Rydberg-Klein-Rees potential function calculations for the ground state ($X^2\Pi$) and excited ($B^2\Sigma^-$) states [137] of methylidyne (CH) radical $^+$. *Models Chem.* **136**, 205–214. [138]
14. Szalay, P.G.; Nemes, L. Tunnelling lifetimes of the rovibronic leveles in the B electronic state of the CH radical obtained from *ab* [139] *initio* data. *Molec. Phys.* **1999**, *96*, 359–366. [140]
15. Hornkohl, J.O.; Nemes, L; Parigger, C.G.; Spectroscopy of Carbon Containing Diatomic Molecules. In *Spectroscopy, Dynamics and* [141] *Molecular Theory of Carbon Plasmas and Vapors: Advances in the Understanding of the Most Complex High-Temperature Elemental System*; [142] Nemes, L., Irle, S., Eds.; World Scientific: Singapore, SG, 2011; Chap. 4, pp. 113–165. [143]
16. Parigger, C.G.; Hornkohl, J.O. *Quantum Mechanics of the Diatomic Molecule with Applications*; IOP Publishing: Bristol, UK, 2020. [144]
17. Parigger, C.G.; Surmick, D.M.; Helstern, C.M.; Gautam, G.; Bol'shakov, A.A; Russo, R. Molecular Laser-Induced Breakdown [145] Spectroscopy, In *Laser Induced Breakdown Spectroscopy*, 2nd ed.; Singh, J.P., Thakur, S.N., Eds.; Elsevier: Amsterdam, The [146] Netherlands, 2020; Chapter 7, pp. 167–212. [147]
18. Parigger, C.G. Diatomic Line Strengths for Fitting Selected Molecular Transitions of AlO, C_2, CN, OH, N_2^+, NO, and TiO, Spectra. [148] *Preprints* **2022**, 2022100410 (doi: 10.20944/preprints202210.0410.v1). [149]

19. Brzozowksi, J.; Bunker, P.; Elander, N.; Erman, P. Predissociation effects in the A, B, and C states of CH and the interstellar formation of CH via inverse predissociation. *Astrophys. J.* **1976**, *207*, 414–424.

20. Erman, P. Time Resolved Spectroscopy of Small Molecules. In *Molecular Spectroscopy Volume 6: A Review of the Literature published in 1977 and 1978*; Barrow, R.F., Long, D.A., Sheridian, J., Eds.; The Royal Society Chemistry: London, UK, 1979; Chap. 5, 174–231.

21. Erman P. Astrophysical Applications of Time Resolved Molecular Spectroscopy. *Phys. Scr.* **1979**, *20*, 575–581.

22. Warnatz, J. *Combustion Chemistry*; Springer: New York, NY, USA, 1984.

23. Raiche, G.A.; Jeffries, J.B. Laser-induced fluorescence temperature measurements in a dc arcjet used for diamond deposition. *Appl. Opt.* **1993**, *32*, 4629–4635.

24. Ubachs, W.; Meijer, G.; ter Meulen, J.J.; Dymanus, A. Hyperfine structure and lifetime of the C $^2\Sigma^+$, $v = 0$ state of CH. *J. Chem. Phys.* **1986**, *84*, 3032–3041.

25. Parigger, C.G.; Woods, A.C.; Surmick, D.M.; Gautam, G.; Witte, M.J.; Hornkohl, J.O. Computation of diatomic molecular spectra for selected transitions of aluminum monoxide, cyanide, diatomic carbon, and titanium monoxide. *Spectrochim. Acta Part B At. Spectrosc.* **2015**, *107*, 132–138.

26. *MATLAB Release R2022a Update 5*; The MathWorks, Inc.: Natick, MA, USA, 2022.

27. Surmick, D.M. (The University of Tennessee, University of Tennessee Space Institute, Tullahoma, TN, USA); Hornkohl, J.O. (The University of Tennessee, University of Tennessee Space Institute, Tullahoma, TN, USA). Private communication, 25 April 2016.

28. Hornkohl, J.O. (The University of Tennessee, University of Tennessee Space Institute, Tullahoma, TN, USA). Private communication, 19 February 2004.